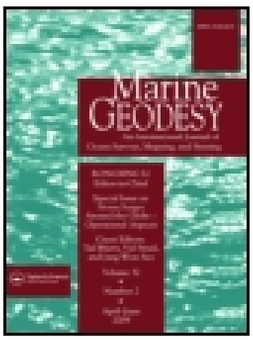

Marine Geodesy

ISSN: 0149-0419 (Print) 1521-060X (Online) Journal homepage: http://www.tandfonline.com/loi/umgd20

# Shoreline Extraction from RADARSAT-2 Intensity Imagery Using a Narrow Band Level Set Segmentation Approach

Yuanming Shu , Jonathan Li & Gary Gomes

**To cite this article:** Yuanming Shu , Jonathan Li & Gary Gomes (2010) Shoreline Extraction from RADARSAT-2 Intensity Imagery Using a Narrow Band Level Set Segmentation Approach, Marine Geodesy, 33:2-3, 187-203, DOI: 10.1080/01490419.2010.496681

**To link to this article:** http://dx.doi.org/10.1080/01490419.2010.496681

*Marine Geodesy*, 33:187–203, 2010

ISSN: 0149-0419 print / 1521-060X online
DOI: 10.1080/01490419.2010.496681

Taylor & Francis
Taylor & Francis Group

# Shoreline Extraction from RADARSAT-2 Intensity Imagery Using a Narrow Band Level Set Segmentation Approach

YUANMING SHU, JONATHAN LI, AND GARY GOMES

Department of Geography and Environmental Management,
Faculty of Environment, University of Waterloo, Waterloo, Ontario, Canada



*This paper presents a semi-automated method for shoreline extraction from RADARSAT-2 intensity imagery. First, a preprocessing is applied to enhance the contrast of the SAR image. Second, thresholding combined with morphological filtering is employed to segment the SAR image into the land and the sea. Third, narrow band level set segmentation is implemented to refine the segmentation result. In the last step, morphological filters are utilized to eliminate any remaining spurious segments. Boundaries between the land and the sea are delineated into shorelines based on the segmentation result. Experiment on RADARSAT-2 intensity images demonstrates that the proposed method is promising.*

**Keywords** Shoreline mapping, RADARSAT-2, level set segmentation, narrow band

## 1. Introduction

Coastal zones are valuable in terms of fisheries, tourism, habitat, and integrity of coastal ecosystems. Sea level rise and erosion are expected to accelerate as a result of global warming, increasing the exposure of coastal zones to storm surges, flooding, and other disasters (Mcinnes et al. 2004). Shoreline mapping and change detection are critical for studies of shoreline landward migration, coastal flood forecasting, the potential impact of tsunamis on safety of navigation, nautical charting, and legal boundary determination (Horritt et al. 2001; Graham et al. 2003; NRC 2004; Polngam et al. 2005; Li et al. 2008; Wang and Allen 2008). The use of earth observation technology has proved a cost-effective approach for shoreline mapping and updating compared to traditional ground survey techniques. The synthetic aperture radar (SAR)-equipped satellite is preferred to the optical one, as it is independent of sunlight and not affected by clouds. However, it has been traditionally limited by the lack of high-spatial resolution SAR sensors. This situation has been changed since 2007, with the new generation of high-resolution SAR imaging satellites, including 1 m X band Italian COSMO-SkyMed, 1 m X band German TerraSAR-X, and 3 m C band Canadian RADARSAT-2.

RADARSAT-2 was launched on December 14, 2007, and provides all imaging modes of RADARSAT-1 as well as some new modes that incorporate significant innovations and improvements (van der Sanden 2004). The capability of RADARSAT-2 to acquire images

Received 20 August 2009; accepted 27 April 2010.
Address correspondence to Dr. J. Li, 200 University Avenue West, Waterloo, Waterloo, Ontario, Canada N2L 3G1. E-mail: junli@uwaterloo.ca

with 3 m spatial resolution in its ultra-fine mode as well as 8 m in fine mode will greatly improve the accuracy of shoreline mapping. Besides, RADARSAT-2 operates in three different polarization modes: the selective single polarization (HH or HV or VH or VV), the selective dual polarization (HH and HV or VV and VH), and the quad polarimetric (HH, HV, VV, VH), also called fully polarimetric mode. HV polarized imagery has been recognized to have a larger waterland contrast than HH polarized imagery (van der Sanden and Ross 2001). The limited effect of wind speed variations on the HV backscatter signal of water also has been confirmed by the results presented in Ufermann and Romeiser (1999). Moreover, polarimetric SAR imagery is expected to have stronger discriminate power between the land and the sea than single polarized SAR imagery (van Zyl 1989; Yu and Acton 2004). Yeremy et al. (2000) also explored the potential of polarimetric SAR for shoreline mapping. All of these new properties of RADARSAT-2 make it an excellent resource for shoreline mapping.



## 2. Related Work

Extraction of shorelines from SAR imagery is facilitated by the large contrast in the backscatter signal as received from sea and land areas (van der Sanden and Ross 2001). The land area usually appears to be light on SAR imagery, while the sea area often appears to be dark. Compared to other shorelines defined in the literature, such as the tide-datum-based shoreline or the interpreted high-water line, the shoreline extracted from SAR imagery is actually the instantaneous land/water interface at the stage of tide when the image is captured. Interested readers are refereed to Boak and Turner (2004) for the discussion of differences between various definitions of shorelines.

Extraction of shorelines from SAR imagery can be done manually or automatically. Compared to automated extraction, the manual approach is time-consuming, labor-intensive, and subjective. Several semi-automated or automated methods for shoreline mapping using SAR imagery have been proposed during the past few years. One of major difficulties for this task is the speckle noises on SAR images. Intensity values may show considerable variability even in the neighborhood of a uniform region (Richards and Jia 2006). To reduce speckle noises, Lee and Jurkevich (1990) first used a sigma filter to smooth the original SAR image. Then, they applied a Sobel edge detector to generate an edge map and used a grey-level thresholding to determine the boundaries between the land and the sea. Lastly, to get closed and connected shorelines, they performed an edge tracing algorithm. As an alternative, Mason and Davenport (1996) used a speckle-sensitive edge detector, a contrast ratio filter detector combined with adaptive edge thresholding and an active contour model for shoreline extraction. Niedermeier et al. (2004) used a more sophisticated technique, wavelet, for edge detection, a blocktracing algorithm to determine the edge, and an active contour to connect edge segments to form continuous shorelines. In consideration of stronger discriminate power between the land and the sea in polarimetric SAR imagery than in a single polarization SAR, Yu and Acton (2004) developed an automated method for shoreline extraction from polarimetric SAR imagery. They used speckle reducing anisotropic diffusion (SRAD) to reduce speckle noises and enhance edges, instantaneous coefficient of variation edge detector for edge detection and watershed segmentation to extract connected shorelines. In the meantime, Dellepiane et al. (2004) proposed a method to extract shorelines from interferometric SAR (InSAR) imagery based on the fuzzy logic method. Liu and Jezek (2004) proposed a comprehensive approach for shoreline extraction, which can be applied to both SAR and optical satellite

images. They used Gaussian filter to reduce noises and anisotropic diffusion operator to enhance major edges along shorelines and suppress other unimportant edges inside land or sea areas. After that, they partitioned the input image into homogenous land and sea regions using locally adaptive thresholding integrated with Canny edge detection and delineated the boundary pixels into shorelines based on the partition. Wang and Allen (2008) used multitemporal SAR data to delineate shorelines based on an edge extraction model to study estuarine shoreline changes in North Carolina (USA).

Though the above methods achieved effective results for shoreline mapping in their experiments respectively, their robustness is affected by the lack of explicit mathematical model for "speckle noise" and "edge." The edge detection operators used in above methods are sensitive to noises, which detects the gradient within a fixed window around the target pixel. Their effectiveness depends on filters to suppress noises to an acceptable degree. However, the use of large filters may blur true boundaries in the meantime. The balance between reducing noises and keeping true boundaries may be difficult to control in practice and needs to be tuned carefully in order to achieve optimal results. Also, the threshold for specifying edges should be chosen carefully. Otherwise, it may generate too many spurious shorelines that are difficult to be eliminated by postprocessing. The pixel-based classification and adaptive thresholding methods mentioned above suffer from the same setbacks as edge-based methods, which are sensitive to noises and dependent on filters.

Instead of filtering out speckle noises, it would be more interesting to model them through statistical methods. Descombes et al. (1996) introduced Markov Random Fields (MRFs) for shoreline mapping from ERS-1 SAR imagery, which is one of popular statistical segmentation models. In the MRFs model, the probability of a pixel belonging to a certain class depends not only on its own feature (e.g., intensity value) but also on the class labels of pixels in its neighbors. For example, if the pixels around the target pixel all belong to a certain class, the target pixel will have a greater chance of belonging to the class. Therefore, the MRFs segmentation model is robust to noises. However, as pointed out by Yu and Clausi (2006), traditional MRFs model is isotropic and unable to preserve filament features. It may fail to work properly in extracting linear feature shorelines. Level set segmentation (Cremers et al. 2007) is another sophisticated method that is easy to incorporate statistical information to model speckle noises during segmentation. Huang et al. (2005) and Karantzalos and Argialas (2008) have successfully used it for oil spill detection from SAR imagery. However, the large computational burden involved with traditional level set methods impedes their further applications to shoreline mapping.

The objective of the study is to develop an effective method for shoreline mapping from RADARSAT-2 intensity imagery. A new method based on narrow band level set segmentation is proposed in this paper. The paper is organized as follows. Section 2 reviews the existing methods for shoreline extraction from SAR imagery. Section 3 gives the background which helps to understand the principle of level set segmentation. Section 4 details the proposed shoreline extraction method. Section 5 shows experimental results applying the proposed method to shoreline extraction from RADARSAT-2 Fine mode intensity imagery with HV polarization and spatial resolution of $8 \times 8$ m. The conclusions and discussions are given in section 6.

## 3. Level Set Segmentation

The level set method is a numerical technique for propagating interfaces, which was introduced by Osher and Sethian (1988). The key idea behind the level set method is to represent $n$ dimensional curve $C$ at time $t$ as the zero level set of $n + 1$dimensional

surface $\phi$,

$$C = \{\vec{x} | \phi(\vec{x}, t) = 0\} \tag{1}$$

and evolve the curve $C$ by solving the partial differential equation (PDE),

$$\begin{aligned} \frac{\partial \phi}{\partial t} &= |\nabla \phi| F \\ \phi(\vec{x}, 0) &= \phi_0(\vec{x}) \end{aligned} \tag{2}$$

where $F$ is the speed in the normal detection. The function $\phi$ is usually defined as a signed distance function because a number of simplifications for curve evolution can be made thereby (Osher and Fedkiw 2002),

$$\begin{aligned} \phi(\vec{x}, t) &= \pm d(\vec{x}), \\ d(\vec{x}) &= \min(|\vec{x} - \vec{x}_C|) \text{ for all } \vec{x}_C \in C \end{aligned} \tag{3}$$

where $d$ is the minimum distance from the point $\vec{x}$ to points on the curve at time $t$. The positive sign is used when the point is outside the curve and the negative is used when the point is inside the curve. As illustrated in Figure 1, the two dimensional (2D) curve $C$ on the bottom row is embedded into a corresponding three dimensional (3D) surface $\phi$ on the top row and represented its zero level set. Compared to the explicit representation by parameterizing the boundary of the curve (Tryggvason et al. 2001), the use of implicit function $\phi$ brings great benefits for curve evolution. It avoids the problems with instabilities, deformation of curve elements, and complicated surgery for topological repair of the curve existing in traditional explicit representation methods (Osher and Fedkiw 2002). Figure 1 illustrates one such advantage using the level set method. In the bottom row, we can see the curve split into two parts during the evolution. It would be difficult for explicit parameterization methods to describe such 2D topology change, as one has to have a surgical procedure to detect such change and then reconstruct parameterization for the two new curves. However, in the top row, the 3D implicit function $\phi$ keeps whole during

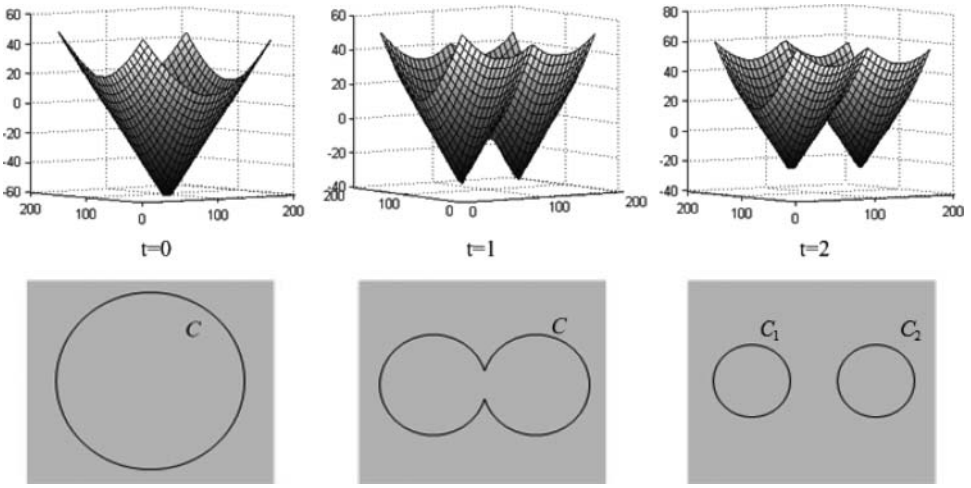


**Figure 1.** Illustration of the level set method.

the evolution. Therefore, it would be much easier to work with the level set function $\phi$ for curve evolution than with the curve directly. Interested readers would be referred to Osher and Fedkiw (2002) for the detailed explanation on other advantages of the level set method. Due to the good properties of the level set function, the level set method has been widely used in image segmentation towards applications to road and building extraction (e.g., Karantzalos and Argialas 2009; Karantzalos and Paragios 2009), highway extraction and vehicle detection (e.g., Niu 2006), and oil spill detection (e.g., Huang et al. 2005; Karantzalos and Argialas 2008).

In terms of the application of the level set method to image segmentation, the 2D contours are represented as the zero level set of 3D signed distance function $\phi$ and evolve by the speed function $F$ according to Eq. (2) until they arrive on the true edges of objects presented in the image. The early speed functions are gradient-based functions (Caselles et al. 1997; Kichenassamy et al. 1995), which will become zero on the edge points characterized by strong gradients. Therefore, the contours will stop when arriving on desired edges of objects. However, these functions have been criticized due to their sensitivities to noises (Chan and Vese 2001). When the image is noisy, contours guided by these functions are easy to trap in local minimum and unable to arrive on desired edges. In consideration of such disadvantages of gradient-based functions, Chan and Vese (2001) proposed a statistical region-based energy function based on Mumford-Shah segmentation technique (Mumford and Shah 1989), which is defined by

$$\begin{aligned} E(c_1, c_2, \phi) = \mu \int_{\Omega} |\nabla H(\phi(x, y))| dxdy + v \int_{\Omega} H(\phi(x, y)) dxdy \\ + \lambda_1 \int_{\Omega} |u_0(x, y) - c_1|^2 H(\phi(x, y)) dxdy + \\ + \lambda_2 \int_{\Omega} |u_0(x, y) - c_2|^2 (1 - H(\phi(x, y))) dxdy \end{aligned} \tag{4}$$

where $\mu$, $v$, $\lambda_1$, $\lambda_2$ are the constants, $u_0(x, y)$ is the image intensity at location $(x, y)$, $c_1$, $c_2$ are the average of image intensities inside and outside the contours, respectively. The Heaviside function $H(\phi) = 0$ for $\phi < 0$ and $H(\phi) = 1$ for $\phi \geq 0$. The first two terms, referred as the prior term, control the smoothness of the contours and inhibit phenomenon of oversegmentation. The last two terms, referred as the data term, measure the total variances inside and outside the contours. Finding the optimal result for image segmentation is equivalent to finding the minimization of the above energy function, which can be achieved by solving the Euler-Lagrange equation

$$\begin{aligned} \frac{\partial \phi}{\partial t} &= -\frac{\partial E}{\partial \phi} \\ \phi(x, y, 0) &= \phi_0(x, y) \end{aligned} \tag{5}$$

where $\phi_0(x, y)$ denotes the initial state of level set function $\phi$.

## 4. Proposed Shoreline Extraction Method

In this paper, a new method for shoreline extraction from RADARSAT-2 intensity imagery is proposed based on narrow band level set segmentation. First, a preprocessing consisting of Gaussian filtering and histogram adjusting is applied to enhance the contrast of the

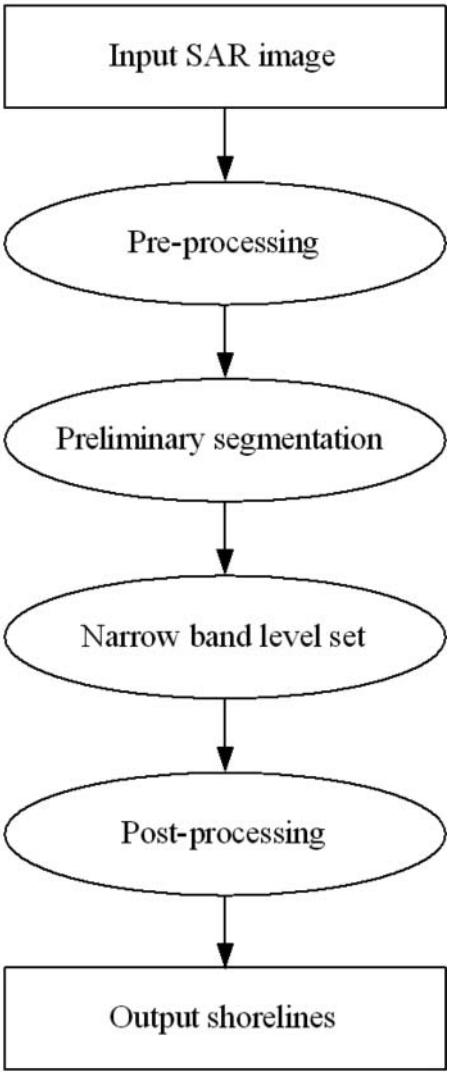


**Figure 2.** Flowchart of the proposed method.



SAR image. Second, thresholding combined with morphological filtering is employed to generate a preliminary segmentation result, which partitions the SAR image into land and sea areas. Third, a narrow band level set segmentation method is implemented to refine the preliminary segmentation result. In the last step, morphological filters are utilized to eliminate any remaining spurious segments. Boundaries between the land and the sea are delineated into shorelines based on the segmentation result. The framework of the proposed method is demonstrated in Figure 2.

### *4.1. Preprocessing*

A $3\times3$ Gaussian filter with standard deviation of 0.5 is utilized to smooth the original SAR image without blurring the edge. Next, a piecewise linear transformation is used to adjust

the histogram of the original image in order to enhance the contrast between the land and the sea areas. The bottom 1% of all pixel values are specified as 0, and the top 1% are specified as 255. The rest of pixels values are stretched within the range from 0 to 255 by a linear transformation. Different from other shoreline extraction methods, the main purpose of preprocessing used here is not to reduce noises to an acceptable level so that the later image processing can work properly but rather for the benefit of manual digitization through visual interpretation, which is discussed in section 5. Extensive experiment shows that narrow band level set segmentation used in our proposed method is robust to noises and can achieve almost the same result for shoreline mapping without preprocessing as the one with preprocessing.

### *4.2. Preliminary Segmentation*

In the level set method, initial contours should be as close as possible to the final segmentation to minimize the time for curve evolution. To achieve this purpose, a preliminary segmentation is implemented by thresholding in intensity domain, which partitions the SAR image into land and sea regions. The intensity threshold can be set by users manually or by automated thresholding methods (e.g., Otsu 1979). Next, morphological filtering including closing and opening operators is applied to the binary image to remove noises and generate a more integrated segmentation result (Gonzalez and Woods 2002). Boundaries between the land and the sea are used as the initial contours for narrow band level set segmentation, which is discussed in the next section.

### *4.3. Narrow Band Level Set Segmentation*

The narrow band method developed by Adalsteinsson and Sethian (1995) is used here to reduce the computational burden involved in traditional level set methods. While the implicit representation of 2D contours into 3D surface brings lots of convenience for curve evolution, it also introduces large computational burden. For a image with size of m by n, a computation labour O(n*m) is required at each iteration in solving Eq. (5) for curve evolution. This will be time-consuming when applied to shoreline mapping, as the SAR image used is usually very large. Instead of evolving level set function in the whole image domain, the narrow band method (see Figure 3) "builds an adaptive mesh around the propagating interface, that

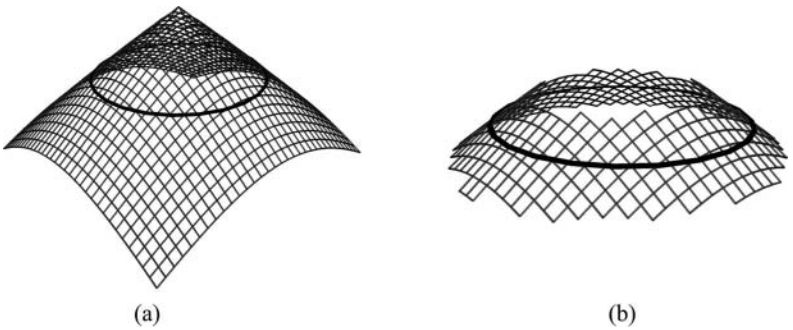


**Figure 3.** Narrow band method. **(a)** Implementation in the whole image domain. **(b)** Implementation in a band close to the zero level set (adapted from Adalsteinsson and Sethain 1995). The black curve is the zero level set.

is, a thin band of neighbouring level sets, and to perform computation only on these grid points" (Adalsteinsson and Sethian 1995). This is appropriate for shoreline extraction, as the number of pixels within a certain distance from contours has already been large enough to obtain good estimations for the average intensity values inside and outside contours as shown in Eq. (4), in order to drive the contours to the true locations of shorelines. In this study, a simplified version of the narrow band method is used for shoreline mapping to further reduce the complexity of programming and increase the computational efficiency. In the original method, the narrow band is reinitialized when the curve is close to the edge of the existing band to keep the curve evolution within the band. Such dynamic updating procedure is useful for applications of the narrow band method in general aspects. However, it is not that necessary for shoreline mapping here, since the locations of shorelines have been roughly given by the preliminary segmentation result as discussed in section 4.2. Therefore, it would be proper to assume that the true locations of shorelines are within a fixed buffer of the initial contours. Besides, to have narrow band update as the curve evolution, one needs a surgery to detect when the curve is about to move out of the band. This will increase computational burden and complex the programming. Moreover, the re-initialization is time-consuming and reveal a disagreement between the level set theory and its implementation (Gomes and Faugeras 2000), which should be avoided. Therefore, we evolve contours in a band with fixed width around the initial contours, even though we may run the risk of missing some shorelines in the process. In practice, users can sacrifice computational time by specifying wider band width in exchange of the higher probability that all shorelines are within the specified band of curve evolution. The detail procedures of narrow band level set segmentation for shoreline extraction are described as follows:

(1) Initial level set function $\phi^0$ using shorelines $C$ obtained in section 4.2 through Eq. (3). Set the width of narrow band $d_0$, maximum iteration time $t_n$ and time interval $\Delta t$. Initial $t = 0$;
(2) Solve Eq. (5) within the narrow band $\{(x, y)||d(x, y, t)| \leq d_0\}$to obtain $\phi^{t+\Delta t}$ from $\phi^t$. $t = t + \Delta t$;
(3) If $t$ is greater than $t_n$ or $\phi$ arrives its stationary, go to step 4. Otherwise, go to step 2; and
(4) Obtain shorelines $C$ by finding points $\{(x, y)|d(x, y, t) = 0\}$.

### *4.4. Postprocessing*

Morphological filtering including closing and opening operators (Gonzalez and Woods 2002) is applied to the binary image after level set segmentation to remove any remaining spurious segments generated due to the effect of speckle noises. Though these segments can be eliminated during the level set evolution without using morphological filters, the computational time will become longer. Next, bright areas inside the sea that are too small to be regarded as islands are removed. Dark holes inside the land are filled, which are probably generated due to the effects of rivers or lakes. In the final step, boundaries between the land and the sea areas are delineated into shorelines based on the segmentation result.

## 5. Experimental Results

An experiment was designed to test the performance of the proposed method by using seven test images. The test data set covers shoreline mapping in different conditions, such as natural shorelines, man-made shorelines, linear feature shorelines, inhomogeneous

land areas, and so on. These images were clipped from an original RADARSAT-2 Fine mode intensity image with HV polarization and spatial resolution of 8 × 8 m, which was acquired over an area in Vancouver, British Columbia, Canada. The size of each test image was 1024 × 1024 pixels.

One test image has been selected to demonstrate the results of the proposed method at each step. Figure 4a shows the test image after preprocessing. As illustrated, the contrast between the land and the sea is enhanced after preprocessing. Figure 4b shows the result of preliminary segmentation. The intensity threshold is set as 50 manually. The radius of morphological opening and closing operators used in this step is set as 3 pixels. The bright area inside the sea with size less than 20 pixels is removed. Dark holes inside the land are filled. Figure 4c shows the result of narrow band level set segmentation. The preliminary

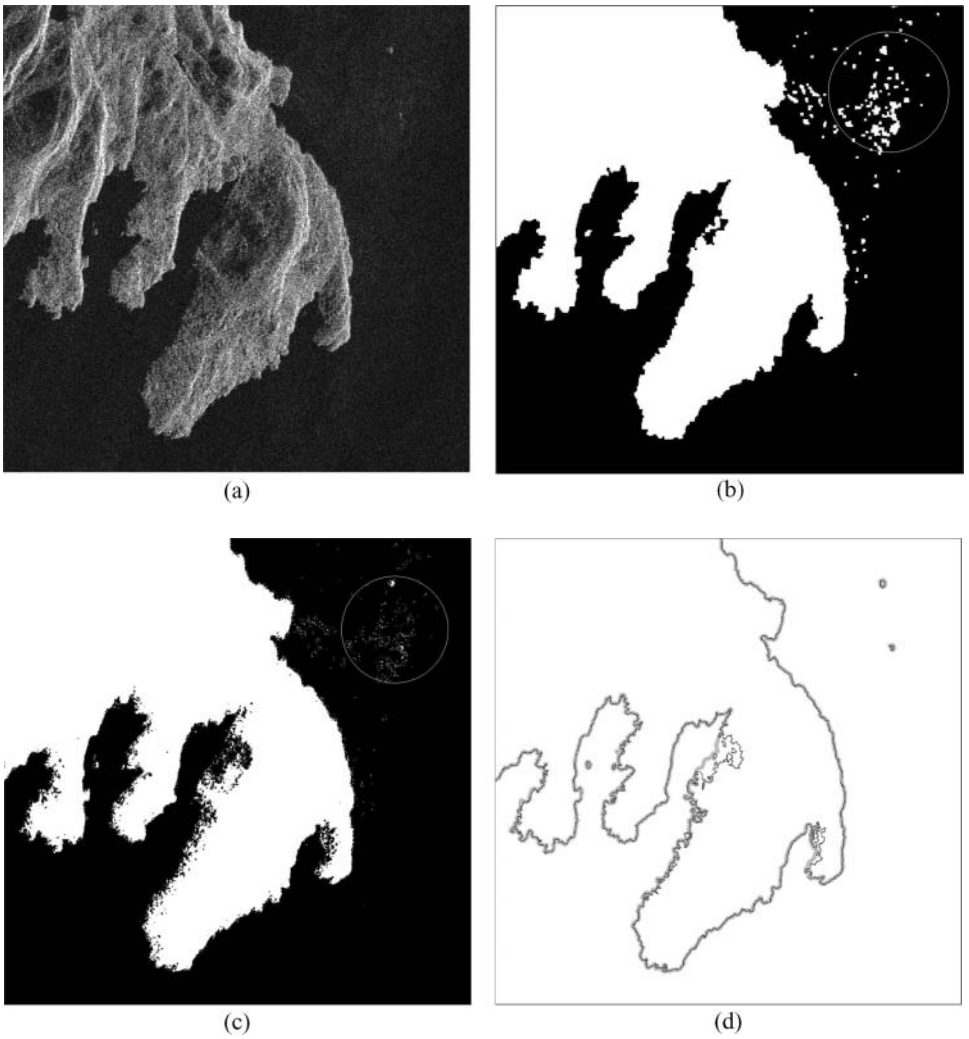


**Figure 4.** Results of the proposed method at each step. **(a)** Original SAR image after pre-processing. **(b)** Preliminary segmentation. **(c)** Narrow band level set segmentation. (d) Final result after postprocessing.

**Table 1**
Intensity threshold (IT) and computational time (CT) for the six test images from (a) to (f) in Figure 5

| | Image (a) | Image (b) | Image (c) | Image (d) | Image (e) | Image (f) |
|---|---|---|---|---|---|---|
| IT | 50 | 50 | 98 | 96 | 70 | 91 |
| CT (seconds) | 26.3 | 25.4 | 10.5 | 18.0 | 17.3 | 19.4 |

segmentation result in Figure 4b is used as initial contours for the level set evolution. Parameters for narrow band level set segmentation are set as: $\lambda_1 = \lambda_2 = 1$, $\mu = 0.05 * 255 * 255$, $v = 0.001 * 255 * 255$, according to the experiment presented by Chan and Vese (2001) when dealing with noisy image. The width of narrow band is set as 50 pixels empirically. The total number of iterations is 20. As shown in Figure 4c, the speckle noises within the white circle of Figure 4b disappeared or became smaller during the evolution, which makes them easier to remove with postprocessing. Figure 4d shows the final result after postprocessing. The radius of the morphological opening and closing operators used in this step is 1 pixel. The bright area inside the sea with size less than 16 pixels is removed. Dark holes inside the land are filled. The gray buffer in Figure 4d represents the layers within 6 pixels of the manually digitized shorelines. The black lines are the final result of computer-extracted shorelines. Visual inspection shows that the result of the proposed method is effective for the test image. The total computational time is 39.6 s on a PC-based MATLAB platform.

Figure 5 shows the experimental results of the other six test images. We used exactly the same parameters for these images as the one described in Figure 4, except for the intensity threshold and the number of iterations of the level set evolution. Table 1 shows the intensity threshold and computational time for each of the six images. The left column of Figure 5 shows the original test images after preprocessing. The right column shows the results of shorelines extraction produced using the proposed method. The gray buffers in images of the right column are the areas within 6 pixels of the manually digitized shorelines. The black lines illustrate the computer-extracted shorelines. Visual inspection shows that the proposed method works well on natural shorelines as shown in Figures 5a and b, man-made shorelines as shown in Figure 5f, linear feature shorelines as shown in Figure 5d, and inhomogeneous land as shown in Figure 5e.

Though there are a total of 15 parameters that need to be set in the proposed method as discussed above, only two parameters need to be tuned in the processing. They are the intensity threshold for preliminary segmentation and the number of iterations for narrow band level set segmentation. Figure 6 illustrates an example of the parameter tuning process. As can be seen from the experimental results, the shoreline extraction result is not that sensitive to the values of intensity threshold. However, properly choosing the threshold will short the computational time of level set evolution.

To quantitatively evaluate the proposed method, a buffer zone approach proposed by Li et al. (2008) is used in this study. The initial idea of the buffer zone approach can be traced back to Wiedeman et al. (1998). The manual on-screen digitizing shoreline is used as the standard line for quantitative accuracy assessment. The commission error is defined by

$$COM = \frac{N_{EL} - N_{ELinMLB}}{N_{EL}} \tag{6}$$

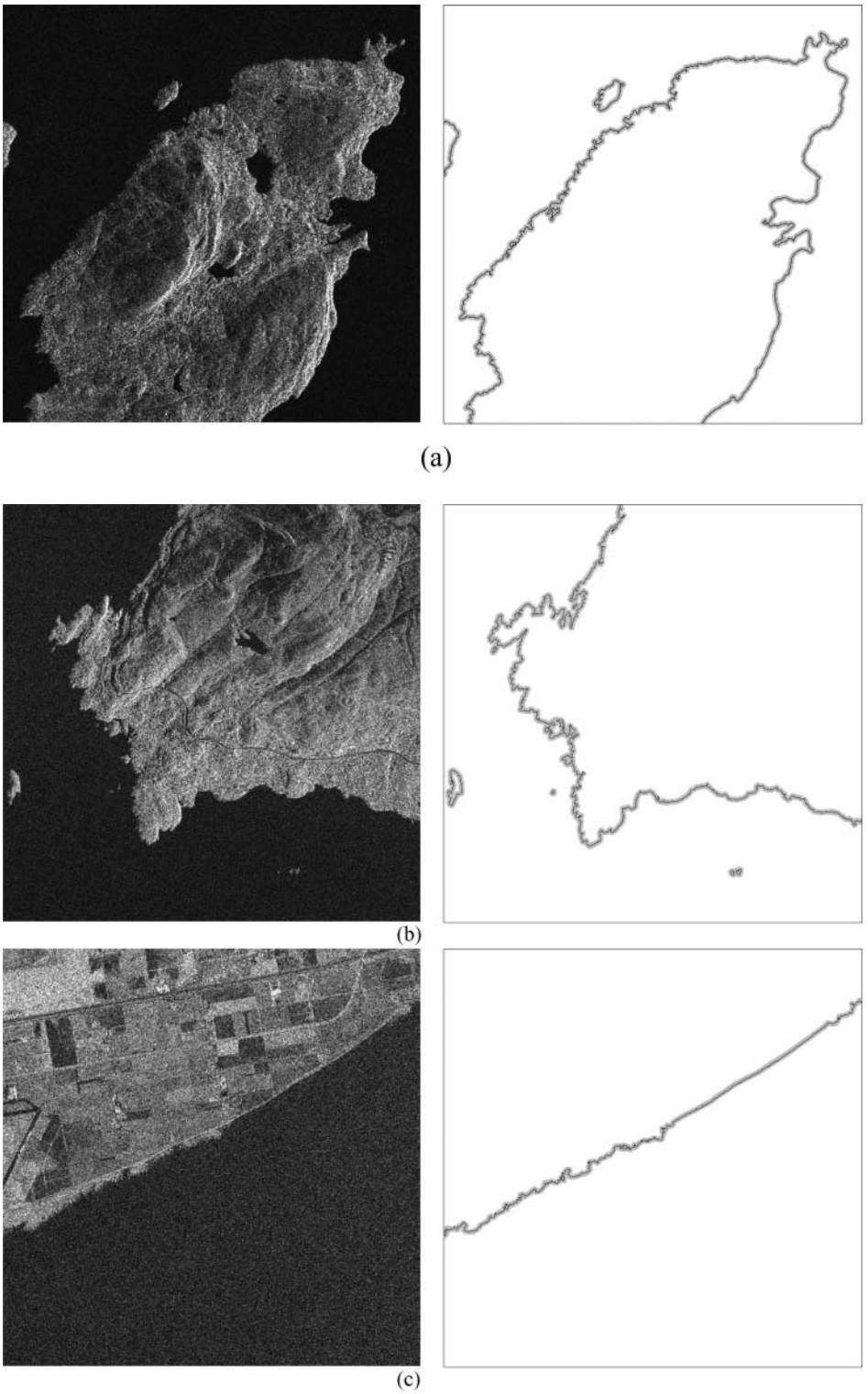


**Figure 5.** Extraction results of the other six test images. *(Continued)*

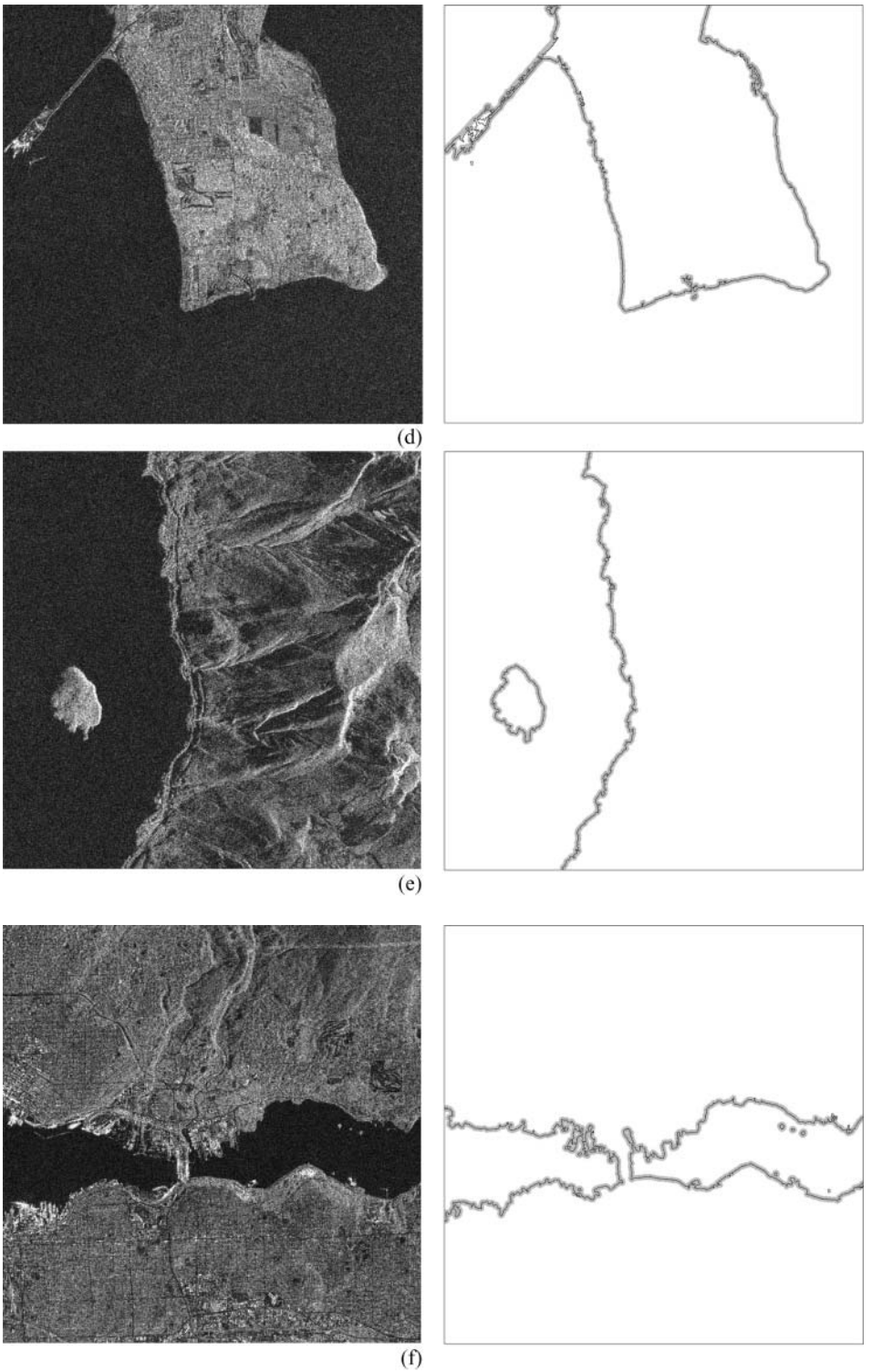

**Figure 5.** (Continued)

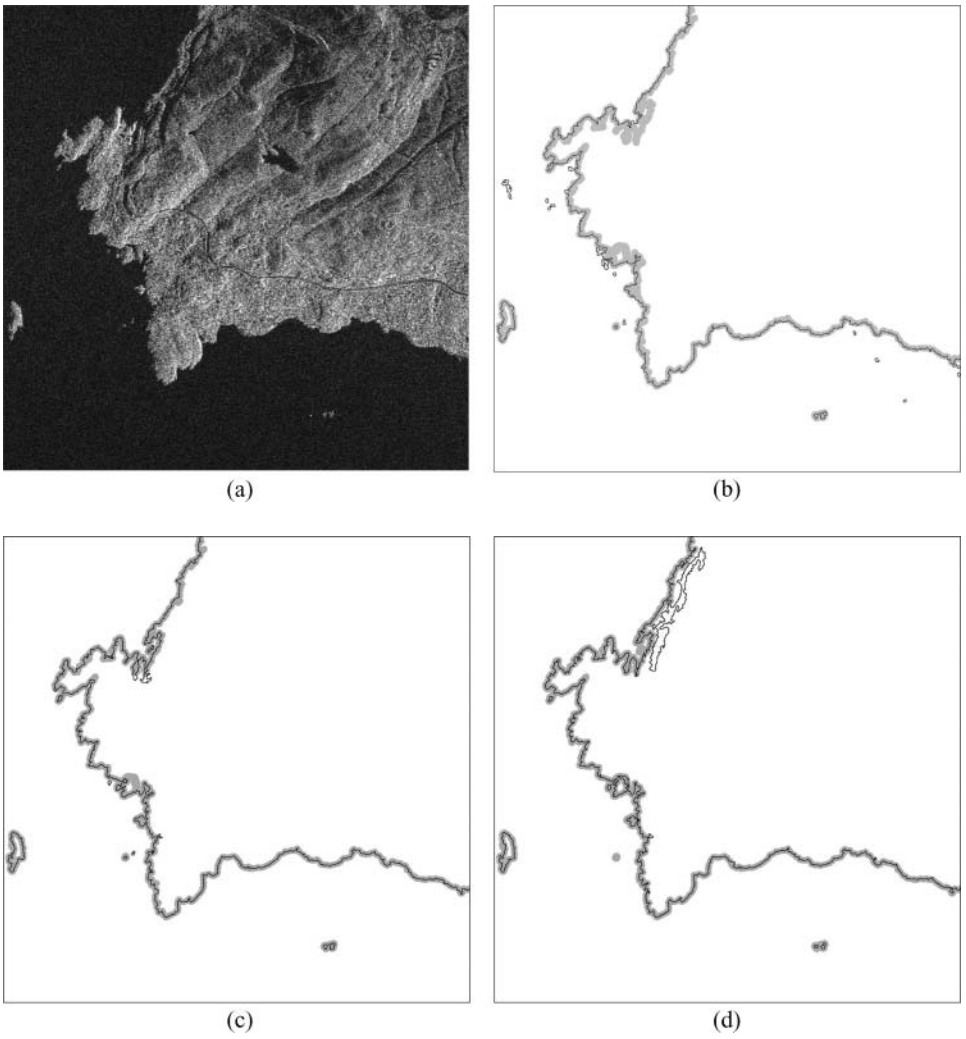


**Figure 6.** Parameter tuning. **(a)** Original SAR image after preprocessing. **(b)** The intensity threshold is 40 and the number of iterations is 100. **(c)** The intensity threshold is 45 and the number of iterations is 80. **(d)** The threshold is 55 and the number of iterations is 20.



where $N_{ELinMLB}$ is the number of pixels on the computer-extracted line within the buffer of the manually digitized shoreline and $N_{EL}$ is the number of pixels on the computer-extracted shoreline. In the work of Li et al. (2008), the omission error was not defined. In this paper, the omission is defined by

$$OM = \frac{N_{ML} - N_{MLinELB}}{N_{ML}} \tag{7}$$

where $N_{MLinELB}$ is the number of pixels on the manually digitized line within the buffer of the computer-extracted shoreline and $N_{ML}$ is the number of pixels on the manually digitized shoreline. The distribution probability of the computer-extracted line on buffer layers for

**Table 2**
Commission errors, omission errors and average errors

| | Max | Min | Mean | Median | Standard Deviation |
|---|---|---|---|---|---|
| COM | 0.1326 | 0.0020 | 0.0308 | 0.0056 | 0.0513 |
| OM | 0.0200 | 0.0000 | 0.0048 | 0.0000 | 0.0082 |
| AE (pixels) | 0.7300 | 0.1400 | 0.3700 | 0.2200 | 0.2664 |

the manually digitized line can be calculated as follows

$$pd(l) = \frac{N_{ELinFLB_l}}{N_{ML}} \tag{8}$$

where $l = 0, 1, 2, \cdots, n$, is the index of buffer layers, $n$ is the total number of buffer layers. $N_{ELinFLB_l}$ is the number of pixels on the computer-extracted line within $l$-th buffer layer. The average error can be calculated by

$$AE = \sum_{l=0}^{n} l * pd(l) \tag{9}$$

Table 2 lists the commission, omission and average errors of each test image calculated by Eqs. (6)–(9). The width of buffer is $n = 4$ pixels in this evaluation. As shown in Table 2, the average error is less than one pixel with standard deviation of 0.2664. The average of commission error is about 3% with standard deviation of 0.0513. The mean average of omission error is 0.48% with standard deviation of 0.0082. The evaluation result shows that the proposed method is accurate for shoreline extraction.

It would be necessary to further identify the areas where poor result occurred and see why the proposed method failed to work properly in those areas. Figure 7 illustrates one

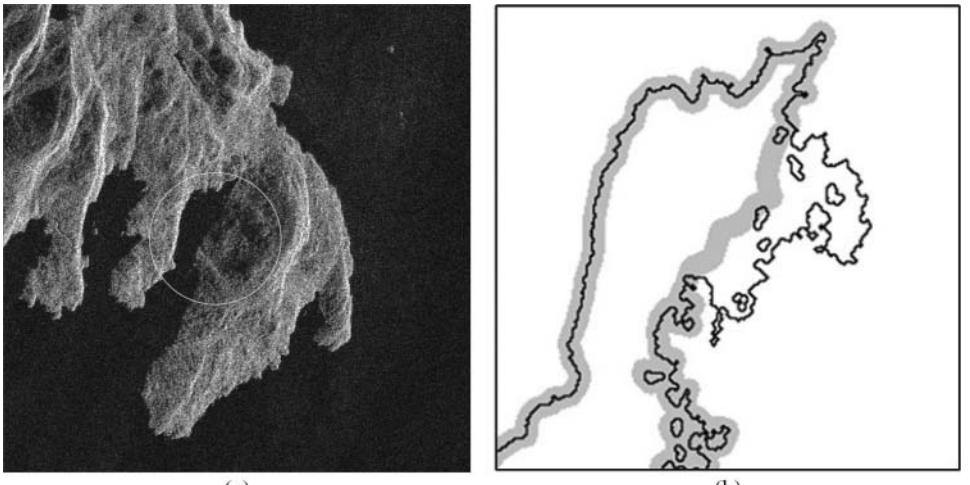


**Figure 7.** Example of poor shoreline extraction. **(a)** Original SAR image after preprocessing. **(b)** Area where the proposed method failed to achieve an effective result.

such example. The reason for the poor extraction is that the intensity within the circle is inhomogeneous due the effect of shadow. Some part of the land appears to be dark and is closer to the appearance of the sea. It indicates edge and texture information should be further incorporated into level set model to achieve effective results in such areas.

## 6. Conclusions and Discussions

In this paper, we have implemented a narrow band level set segmentation method to extract shorelines along the Canadian Pacific coast from RADARSAT-2 Fine mode intensity imagery with HV polarization and spatial resolution of $8 \times 8$ m. A total of seven images were used to test the proposed method. Visual inspection indicated that the proposed method worked well. To quantitatively assess the performance of the proposed method, manual on-screen digitizing shorelines were created and used as the standard lines. The buffer zone approach was utilized to perform the quantitative assessment. For the overall test dataset, the average error was less than one pixel. The average commission and omission errors were 3.08% and 0.48%, respectively, as referred to the manual on-screen digitizing shorelines. It also indicated from the experiment that the use of the preliminary segmentation result as the initial contours of level set, and the narrow band method for propagating level set, largely reduced the computational burden and improved extraction efficiency. Compared to pixel-based methods, region-based method models speckle noise using statistical methods so that is robust to parameters. During the experiment, only the values of intensity threshold and the number of iterations need to be tuned to get a good preliminary segmentation result. Compared to the general isotropic MRF model, the level set segmentation method does not have local assumption about the relationship between surrounding pixels. Therefore, it would favor extraction of the linear feature shorelines as well, which has been illustrated in the experiment. It can also be noticed that the proposed method may be applied to shoreline mapping and updating using interferometry, polarimetric, or multipolarization SAR images. Furthermore, the framework of level set segmentation can easily incorporates edge and texture information (as data term) for extraction (Cremers et al. 2007), which will help overcome adverse effects of winds and shadows and further increase the accuracy of shoreline extraction. These issues will be addressed in our future work.



## Acknowledgements

The authors would like to thanks the three anonymous reviewers for their valuable comments and suggestions.

## References

Adalsteinsson, D., and J. A. Sethian. 1995. A fast level set method for propagating interfaces. *Journal of Computational Physics* 118:269–277.

Boak, E. H., and I. L. Turner. 2004. Shoreline definition and detection: a review. *Journal of Coastal Research* 21:688–703.

Caselles, V., R. Kimmel, and G. Sapiro. 1997. Geodesic active contours. *International Journal of Computer Vision* 22:61–79.

Chan, T. F., and L. A. Vese. 2001. Active contours without edges. *IEEE Transactions on Image Processing* 10:266–277.

Cremers, D., M. Rousson, and R. Deriche. 2007. A review of statistical approaches to level set segmentation: Integrating color, texture, motion and shape. *International Journal of Computer Vision* 72:195–215.

Dellepiane, S., R. D. Laurentiis, and F. Giordano. 2004. Shoreline extraction from SAR images and a method for the evaluation of the shoreline precision. *Pattern Recognition Letters* 25:1461–1470.

Descombes, X., M. Moctezuma, H. Maître a, and J. P. Rudant. 1996. Coastline detection by a Markovian segmentation on SAR images, *Signal Processing* 55:123–132.

Graham, D., M. Sault, and J. Bailey. 2003. National ocean service shoreline–past, present, and future. *Journal of Coastal Research* SI:14–32.

Gomes, J., and O. Faugeras. 2000. Reconciling distance functions and level sets. *Journal of Visual Communication and Image Representation* 11:209–223.

Gonzalez, R. C., and R. E. Woods. 2002. *Digital image processing* (2nd ed.). Upper Saddle River, NJ: Prentice Hall.

Horritt, M. S., D. C. Mason, and A. J. Luckman. 2001. Flood boundary delineation from synthetic aperture radar imagery using a statistical active contour model. *International Journal of Remote Sensing* 22:2489–2507.

Huang, B., H. Li, and X. Huang. 2005. A level set method for oil slick segmentation in SAR images. *International Journal of Remote Sensing* 26:1145–1156.

Karantzalos, K., and D. Argialas. 2009. A region-based level set segmentation for automatic detection of man-made objects from aerial and satellite images. *Photogrammetric Engineering & Remote Sensing* 75:667–678.

Karantzalos, K., and N. Paragios. 2009. Recognition-driven two-dimensional competing priors toward automatic and accurate building detection. *IEEE Transactions on Geoscience and Remote Sensing* 47:133–144.

Karantzalos, K., and D. Argialas. 2008. Automatic detection and tracking of oil spills in SAR imagery with level set segmentation. *International Journal of Remote Sensing* 29:6281–6296.

Kichenassamy, S., A. Kumar, P. J. Olver, A. Tannenbaum, and A. J. Yezzi. 1995. Gradient flows and geometric active contour models. *IEEE International Conference on Computer Vision*, June 20–June 20, Boston, MA.

Lee, J., and I. Jurkevich. 1990. Shoreline detection and tracing in SAR images. *IEEE Transactions on Geoscience and Remote Sensing* 28:662–668.

Li, Y., J. Li, and Y. Lu. 2008. A fuzzy segmentation-based approach to extraction of shorelines from IKONOS imagery. *Geomatica* 62:407–417.

Liu, H., and K. C. Jezek. 2004. Automated extraction of shoreline from satellite imagery by intergrating Canny edge detection and locally adaptive thresholding methods. *International Journal of Remote Sensing* 25:937–958.

Mason, D. C., and I. J. Davenport. 1996. Accurate and efficient determination of the shoreline in ERS-1 SAR images. *IEEE Transactions on Geoscience and Remote Sensing* 34:1243–1253.

Mattar, K. E., and L. Gallop. 2003. Arctic shoreline delineation & feature detection using RADARSAT-1 interferometry: Case study over Alert. http:// pubs.drdc.gc.ca/PDFS/unc17/p520801.pdf

Mcinnes, K. L., K. J. E. Walsh, G. D. Hubbert, and T. Beer. 2004. Impact of sea-level rise and storm surges on a coastal community. *Natural Hazards* 30:187–207.

Mumford, D., and J. Shah. 1989. Optimal approximation by piecewise smooth functions and associated variational problems. *Communications on Pure Applied Mathematics* 42:577–685.

National Research Council (NRC). 2004. *A geospatial framework for the coastal zone: National needs for coastal mapping and charting*. Washington, DC: National Academy Press, pp. 41–48.

Niedermeier, A., E. Romaneeßen, and S. Lehner. 2004. Detection of shorelines in SAR images using wavelet methods. *IEEE Transactions on Geoscience and Remote Sensing* 38:2270–2281.

Niu, X. 2006. A semi-automatic framework for highway extraction and vehicle detection based on a geometric deformable model. *ISPRS Journal of Photogrammetry and Remote Sensing* 61:170–186.

Osher, S. J., and R. Fedkiw. 2002. Level set methods and dynamic implicit surfaces. *Applied Mathematical Science*, vol. 153. Berlin: Springer-Verlag.

Osher, S., and J. A. Sethian. 1988. Fronts propagating with curvature-dependent speed: Algorithms based on Hamilton-Jacobi formulations. *Journal of Computational Physics* 79:12–49.

Otsu, N. 1979. A threshold selection method from gray-level histograms. *IEEE Transactions on Systems, Man, and Cybernetics* 9:62–66.

Polngam, S., T. Sanguantrakool, E. Pricharchon, and S. Phoompanich. 2005. Remote sensing technology for tsunami disasters along the Andaman Sea, Thailand. *Proceedings of the 3rd International Workshop on Remote Sensing for Post-Disaster Response*, September 12–13, Chiba, Japan.

Richards, J. A., and X. Jia. 2006. *Remote Sensing Digital Image Analysis* (4th ed.). Berlin: Springer-Verlag.

Sethian, J. A. 1999. *Level set methods and fast marching methods*. Cambridge, UK: Cambridge University Press.

Touzi, R., A. Lopes, and P. Bousquet. 1988. A statistical and geometrical edge detector for SAR images. *IEEE Transactions IEEE Transactions* 26:764–773.

Tryggvason, G., B. Bunner, D. Juric, W. Tauber, S. Nas, J. Han, N. Al-Rawahi, and Y.-J. Jan. 2001. A front tracking method for the computations of multiphase flow. *Journal of Computational Physics* 169:708–759.

Ufermann, S., and R. Romeiser. 1999. A new interpretation of multifrequency/ multipolarization radar signatures of the Gulf Stream front. *Journal of Geophysical Research* 104:25697–25705.

Van Der Sanden van, J. J., and S. G. Ross. 2001. Applications potential of RADARSAT-2: A preview. Unpublished report, Canada Centre for Remote Sensing.

Van Der Sanden, J. J. 2004. Anticipated applications potential of RADARSAT-2 data. *Canadian Journal of Remote Sensing* 30:369–379.

van Zyl, J. J. 1989. Unsupervised classification of scattering behavior using radar polarimetric data. *IEEE Transactions on Geoscience and Remote Sensing* 27:36–45.

Wang, Y., and T. R. Allan. 2008. Estuarine shoreline change detection using Japanese ALOS PALSAR HH and JERS-1 L-HH SAR data in the Albemarle-Pamlico Sounds, North Carolina, USA. *International Journal of Remote Sensing* 29:4429–4442.

Wiedemann, C., C. Heipke, H. Mayer, and O. Jamet. 1998. Empirical evaluation of automatically extracted road axes. In *Empirical evaluation methods in computer vision*, eds. K. Bowyer and P. Phillips, 172–187. Silver Spring, MD: IEEE Computer Society Press.

Yeremy, M., J. D. Beaudoin, G. M. Walter, and A. Beaudoin. 2000. Shoreline mapping from SAR imagery: A polarimetric approach. *In Proceedings of the 22nd In Proceedings of the 22nd*, August 21–25, Victoria, Canada.

Yu, Y., and S. T. Acton. 2002. Speckle reducing anisotropic diffusion. *IEEE Transactions on Geoscience and Remote Sensing* 11:1260–1270.

Yu, Y., and S. T. Acton. 2004. Automated delineation of shoreline from polarimetric SAR imagery. *International Journal of Remote Sensing* 25:3423–3438.

Yu, Q., and D. Clausi. 2006. Filament preserving model (FPM) segmentation applied to SAR sea-ice imagery. *IEEE Transactions on Geoscience and Remote Sensing* 44:3687–3694.